

Microstructural, magnetic and dielectric performance of rare earth ion (Sm^{3+})-doped MgCd ferrites

Dandan Wen(文丹丹), Xia Chen(陈霞), Dasen Luo(骆大森), Yi Lu(卢毅),Yixin Chen(陈一鑫), Renpu Li(黎人溥), and Wei Cui(崔巍)

Citation: Chin. Phys. B, 2022, 31 (**7**): 078503. DOI: 10.1088/1674-1056/ac398c
Journal homepage: http://cpb.iphy.ac.cn; http://iopscience.iop.org/cpb

What follows is a list of articles you may be interested in

Experimental and computational study of visible light-induced photocatalytic ability of nitrogen ions-implanted TiO_2 nanotubes

Ruijing Zhang(张瑞菁), Xiaoli Liu(刘晓丽), Xinggang Hou(侯兴刚), Bin Liao(廖斌)
Chin. Phys. B, 2020, 29 (**4**): 048501. DOI: 10.1088/1674-1056/ab6d53

Homogeneous and inhomogeneous magnetic oxide semiconductors

Xiao-Li Li(李小丽), Xiao-Hong Xu(许小红)
Chin. Phys. B, 2019, 28 (**9**): 098506. DOI: 10.1088/1674-1056/ab38ac

Tunable broadband metamaterial absorber consisting of ferrite slabs and a copper wire

Yang Yong-Jun,Huang Yong-Jun,Wen Guang-Jun,Zhong Jing-Ping,Sun Hai-Bin
Chin. Phys. B, 2012, 21 (**3**): 038501. DOI: 10.1088/1674-1056/21/3/038501

Microstructural, magnetic and dielectric performance of rare earth ion (Sm^{3+})-doped MgCd ferrites

Dandan Wen(文丹丹)[1,2,3,†], Xia Chen(陈霞)[3], Dasen Luo(骆大森)[3], Yi Lu(卢毅)[1], Yixin Chen(陈一鑫)[3], Renpu Li(黎人溥)[1], and Wei Cui(崔巍)[3,‡]

[1] *Doctoral Research Station of Chongqing Key Laboratory of Optoelectronic Information Sensing and Transmission Technology, Chongqing University of Post and Telecommunications, Chongqing* 400065, *China*

[2] *State Key Laboratory of Electronic Thin Films and Integrated Devices, University of Electronic Science and Technology of China, Chengdu* 610054, *China*

[3] *Chongqing Key Laboratory of Autonomous Navigation and Microsystem, Chongqing University of Post and Telecommunications, Chongqing* 400065, *China*

(Received 8 September 2021; revised manuscript received 4 November 2021; accepted manuscript online 15 November 2021)

The combined effects of Sm^{3+} substitution together with the addition of 3 wt% Bi_2O_3 endow MgCd ferrites with excellent magnetic permeability and dielectric permittivity. Various concentrations of Sm^{3+} ($x = 0$, 0.03, 0.06, 0.09, 0.12 and 0.15) were employed to modify the permeability (μ') and permittivity (ε') of the MgCd ferrites. X-ray diffraction, scanning electron microscopy (SEM), vibrating sample magnetometry and vector network analysis techniques were used to characterize the samples. The measurement results reveal that the ferrites processed a saturation magnetization of up to 36.8 emu/g and coercivity of up to 29.2 Oe via the conventional solid-state reaction method. The surface morphology SEM confirms that with increasing Sm^{3+} concentration, the grain shape changes from a polygon to a circle. Moreover, the dielectric permittivity can reach a value of 23. The excellent properties obtained in Sm^{3+}-substituted Mg ferrites suggest that they could be promising candidates for modern high-frequency antenna substrates or multilayer devices.

Keywords: ferrites, Sm^{3+} ions, substitution, magnetic permeability, dielectric permittivity

PACS: 85.70.Ge, 81.40.–z **DOI:** 10.1088/1674-1056/ac398c

1. Introduction

With the advent of the 5G era, functional ceramic materials will usher in a new round of rapid development. Ferrites, as functional ceramics, have been extensively used in modern electronic technologies, making them one of the most significant magnetic materials.[1–3] Around the world, ferrite development and research has been very active, and its progress promotes the rapid development of high-tech industries such as electronics, information, machinery, aerospace, communication and the chemical industry.[4–6] Soft ferrite materials not only possess spontaneous magnetization and electrical properties with chemical and thermal stability but are also pertinent magnetic materials having high permeability with low loss, high resistivity, low cost and high mechanical hardness.[7–9] Recently, Mg-based ferrites ($MgFe_2O_4$) have been widely studied for their spinel structure, and show interesting structural, electrical and sensing properties.[10,11] The Cd-substituted $MgFe_2O_4$ system shows a canted spin arrangement on octahedral B-sites such as Cd-substituted mixed ferrites, for example Cu–Cd,[12] Li–Cd,[13] and Ni–Cd.[14] Gadkari *et al.* reported $Mg_{1-x}Cd_xFe_2O_4$ ($x = 0$, 0.2, 0.4, 0.6, 0.8 and 1) with the addition of 5% Y^{3+} or Sm^{3+} by the oxalate co-precipitation technique.[15–17] They investigated the structural, magnetic and DC electrical performance of the $MgCdFe_2O_4$ system by means of x-ray diffraction (XRD) and magnetic and electrical measurements. They also used Mg–Cd ferrites as gas sensors to detect liquid petroleum gas, Cl_2 and C_2H_5OH. Although Mg–Cd ferrites with different cadmium contents have been researched, compared with other widely studied ferrites there is more to be understood.

It is known that the addition of rare earth elements to ferrites can result in the modification of structural, electrical and magnetic properties.[18–22] Many research groups have researched the effect of rare earth cations in different ferrites to tailor their microstructural, electric and magnetic properties. Bhosale *et al.* extensively studied the effect of the addition of Gd^{3+} on the electric and magnetic properties of Mg–Cd ferrite, and the phenomenon of an increase in the lattice constant with increasing Cd^{2+} content was discovered.[20] Wu *et al.* investigated the effects of RE^{3+}-substituted cobalt ferrite $CoFe_{1.9}RE_{0.1}O_4$ (RE = Pr^{3+}, Sm^{3+}, Tb^{3+}, Ho^{3+}) on structural, magnetic and adsorption properties through XRD, transmission electron microscopy, energy dispersive spectroscopy, Fourier transform infrared (FTIR) spectroscopy, Raman spectroscopy and vibrating sample magnetometry.[21] The results indicate that the RE^{3+} substitution leads to a decrease in the particle size, magnetization and coercivity of the $CoFe_2O_4$ ferrite. The effect of doping with different rare earth elements on

†Corresponding author. E-mail: wendd@cqupt.edu.cn
‡Corresponding author. E-mail: cuiwei@cqupt.edu.cn

© 2022 Chinese Physical Society and IOP Publishing Ltd

spinel Mn–Cr ferrite has been studied by Abdellatif *et al.* They found that substituted rare earth ions distort the octahedral and tetrahedral sites of the ferrite lattice.[22]

In this paper, we report the effect of Sm^{3+} substitution on the structural, magnetic and electrical properties of Mg–Cd ferrites prepared by the solid-state sintering method. In this work, Sm^{3+} was substituted intensively at low to high concentrations (0.15), and there were no additional phases in the spinel structure.

2. Experiments

Sm-doped Mg–Cd ferrite with the chemical composition $Mg_{0.8}Cd_{0.2}Fe_{2-x}Sm_xO_4$ ($0 \leq x \leq 0.15$, in steps of 0.03) was synthesized through a solid-state reaction method at high temperature. The pure raw material powders (MgO, CdO, Sm_2O_3 and Fe_2O_3) were weighed according to their respective stoichiometric ratios and then mixed and ball milled in a planetary mixer with zirconia balls for 18 h. Afterwards, the well-mixed powder was dried and presintered at 1150 °C in air for 4 h. The preliminary sintered powder with 3 wt% Bi_2O_3 was ball milled again in deionized water for another 18 h. After the addition of 8 wt% polyvinyl alcohol (PVA) as a binder, the dried powder then ground into particles. High pressure, up to 10 MPa, was applied to press the particles into 2 mm–3 mm thick circular plates. Finally, the molded samples were sintered at 925 °C in air for 6 h.

The crystallography of the samples was measured using XRD (DX-2700, Haoyuan Co., China) with Cu-$K\alpha$ radiation at a θ–2θ geometric angle from 10° to 70°. The microtopography was captured by scanning electron microscopy (SEM; JEOL JSM-6490, Japan). The magnetization hysteresis loops were obtained using a vibrating sample magnetometer (model BHL-525, Japan) with a direct current magnetic field of ±2500 Oe. Saturation magnetization and coercivity were calculated from the *M*–*H* loops. The complex magnetic permeability and dielectric permittivity were measured using an Agilent 4991 impedance analyzer (Agilent Technologies, Palo Alto, CA, USA) at various frequencies ranging from 1 MHz to 1 GHz. The bulk density was measured using Archimedes' principle in an autodensity tester (GF-300D, AND Co.). All measurements were carried out at room temperature.

3. Results and discussion

The XRD patterns of $Mg_{0.8}Cd_{0.2}Fe_{2-x}Sm_xO_4$ ($x = 0$, 0.03, 0.06, 0.09, 0.12, and 0.15) with added Sm^{3+} are displayed in Fig. 1. The diffractogram reveals that all the samples crystallized in a normal spinel structure indexed to standard $MgFe_2O_4$ peaks, referred to as standard PDF card file No. 17-0464. From Fig. 1(a), all the diffraction peaks are in good agreement with the indexed peaks, while no impurity phases were detected, indicating that the phase formation of $Mg_{0.8}Cd_{0.2}Fe_{2-x}Sm_xO_4$ was not interfered with by Sm_2O_3 and Bi_2O_3 oxide. When $x = 0$ and $x = 0.03$, there was a small amount of $\alpha = Fe_2O_3$ (JCPDS 33-0664) phase in these two samples. The reason for this was uneven mixing during the preparation process. Moreover, a slight shift of the diffraction peaks to a low angle is observed as x increases from 0 to 0.15, similar to the enlarged figure of the main peak shown in Fig. 1(b). For the main peak [(311)] toward the left, this is due to the increase in the lattice constant as the ionic radius of Sm^{3+} increases compared with Fe^{3+}, and the Sm^{3+} concentration increases. In the case of spinel ferrite, the octahedral sublattice (B-site) contains 16 sites, twice as many as the tetrahedral sublattice (A-site), and is the dominant sublattice. Because Fe^{3+} (ionic radius 0.645 Å) in the B-site is substituted by the larger ion Sm^{3+} (ionic radius 0.958 Å), substituting Sm^{3+} causes expansion of the lattice in the B-site, which leads to the diffraction peak shifting overall to the left. Similar research, such as ion doping Mg–Cd[16,20] and Li–Zn,[23] has been reported.

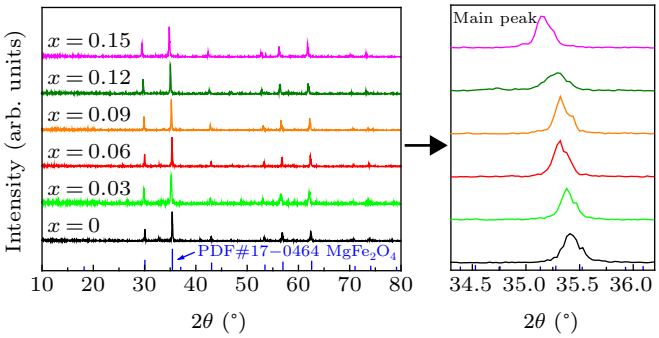


Fig. 1. The XRD patterns of Sm-doped MgCd ferrites with different Sm^{3+} contents.

The increase in bulk density first increases with Sm^{3+} content from 4.552 g/cm^3 to 4.703 g/cm^3 and then remains stable, as shown in Fig. 2(a). This is because the bulk density is related to the lattice constant and lattice distortion. Lattice constants are calculated using Bragg's law as a function of Sm^{3+} content in Mg–Cd ferrites, which is shown in Fig. 2(b). Moreover, the lattice constant shows nonlinear behavior and increases from 8.375 Å to 8.415 Å with increasing Sm^{3+} content, as shown in Fig. 2(b), which may be attributed to the larger ionic radius of Sm^{3+} (0.958 Å) compared with Fe^{3+} (0.645 Å). In the Sm-substituted Mg–Cd spinel structure, all Cd^{2+} occupies the tetrahedral A-site and Sm^{3+} occupies the octahedral B-site. Similar behavior was observed in Mg–Cd ferrite with added Sm^{3+}, suggesting that rare earth ions occupied the octahedral B-site.[15] Additionally, the grain size and pores among grains can also affect the bulk density, as shown in Fig. 3. Noticeably, the lattice constant and bulk density are important factors in the magnetic and dielectric properties of ferrites.

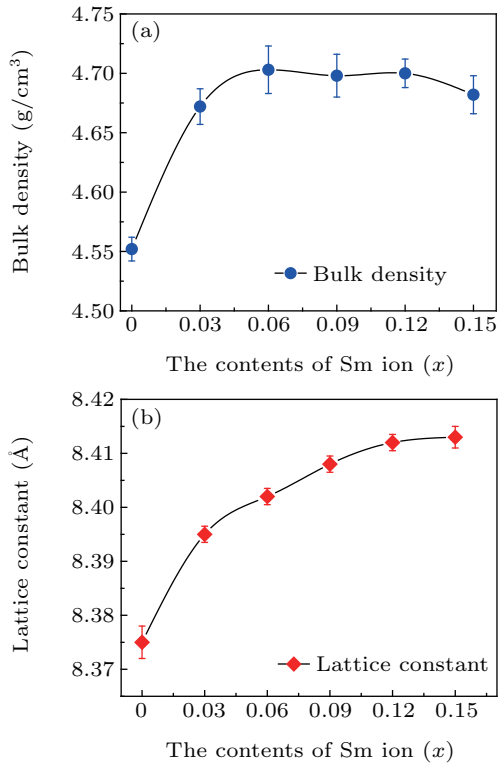


Fig. 2. Dependence of bulk density (a) and lattice constant (b) on Sm^{3+} content.

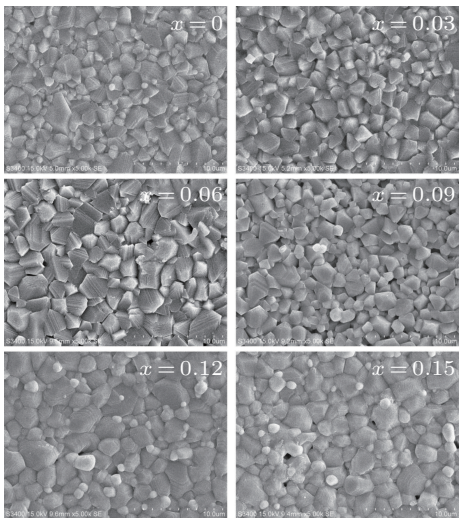


Fig. 3. SEM images of samples with different Sm^{3+} ion contents.

Figure 3 shows SEM images of Mg–Cd ferrites with different amounts of added Sm^{3+} ($x = 0$–0.15). It can be concluded that all the Sm-substituted Mg–Cd ferrites have a relatively homogeneous grain distribution. The particle morphology is cubical, and the grain growth accelerates as x increases from 0 to 0.06. Sm^{3+} has a larger ionic radius than Fe^{3+}, which can explain this phenomenon. For $x \geq 0.12$, the degree of Sm^{3+} substitution leads to a further increase in the grain size of the ferrite, and a few grain pores begin to appear. Meanwhile, the grain shape gradually changes from polygonal polyhedron to arc polyhedron, and some grains even become spherical. The increase in grain size and the appearance of pores cause the magnetic properties of ferrite to deteriorate, but the dielectric properties are improved. Remarkably, almost all the particle morphology remains polyhedral and the grain size is roughly uniform when $x = 0.06$, which gives Sm-substituted Mg–Cd ferrite the best magnetic and dielectric performance.

Figure 4(a) shows the hysteresis loops of the Mg–Cd ferrites with added Sm^{3+} at room temperature. The M–H loops of all samples have narrow hysteresis, which displays excellent soft magnetic characteristics. The saturation magnetization and coercivity, derived from the M–H loops, are also displayed in Fig. 4(b). These results are in close agreement with another report for Mg–Cd ferrite.[16] From Fig. 4, it is apparent that the saturation magnetization increases first from 33.8 emu/g ($x = 0$) to the maximum value of 36.8 emu/g ($x = 0.06$) and then decreases with a further increase in x until the minimum value of 22.7 emu/g is obtained at $x = 0.15$. Evidently, magnetization is relatively dependent on the Sm^{3+} concentration. This is due to the different magnetic moments between the A and B sublattices, depending on their respective cation distributions. It has been reported that in Sm-supplemented Mg–Cd ferrites, all divalent Cd^{2+} ions occupy the tetrahedral A-site and Sm^{3+} ions occupy the octahedral B-site. Mg^{2+} and Fe^{3+} ions occupy the A-sites and B-sites at random. The total magnetization M_s can be expressed as

$$M_s = M_B \cos \alpha_{Y-K} - M_A, \tag{1}$$

where M_B and M_A are the magnetic moments of the A- and B-sites, respectively, and α_{Y-K} is the Yafet–Kittel angle. Using the triangle spin arrangement model to calculate the Yafet–Kittel angle can help us understand the degree of spin canting. α_{Y-K} decreases with Sm^{3+} substitution for $x \leq 0.06$ and there is an increase in the magnetization of the ferrite. Similar results are found in other works based on FTIR results.[16] In addition, the increase in saturation magnetization is also related to the increase in bulk density. The density increased when x increased 0 to 0.06 (Fig. 2(a)), contributing to the saturation magnetization. For $x > 0.06$, the great mass of paramagnetic Sm^{3+} ions would further replace Fe^{3+} in B-sites. However, a small number of Sm^{3+} ions would prefer to occupy A-sites, leading to a decrease in the magnetic moment n_B of ferrite, and hence the total M_s would decrease.

However, as shown in Fig. 4(b), the coercivity gradually decreases and then increases sharply with increasing Sm^{3+} concentration, which displays an inverse trend compared with M_s. The coercivity first decreases from 33.6 Oe (at $x = 0$) to 29.2 Oe (at $x = 0.06$) and then increases to 36.1 Oe (at $x = 0.15$). Brown's relation could explain this behavior:

$$H_c = \frac{2K_1}{\mu_0 M_s}, \tag{2}$$

where K_1 is the crystalline anisotropy constant. The amount of Fe^{3+} decreases because of the increasing Sm^{3+} content on the B-site. Generally, the anisotropy field of ferrites is caused by the presence of Fe^{3+}.[24] In other words, as the Sm^{3+} content increases, the anisotropy constant decreases, and the magnitude of coercivity also decreases when $x < 0.06$. With a further increase in Sm^{3+}, the coercivity increases sharply. This is because the Sm–Fe interaction is stronger than the Sm–Sm interaction on the B-site. In addition, according to Eq. (2), the coercivity is positively proportional to the anisotropy constant and inversely proportional to M_s. Therefore, the coercive force increases with decreasing M_s and increasing K_1 when $x > 0.06$. Moreover, the coercivity is also influenced by the internal stress. When the Sm^{3+} ions enter the spinel lattice, due to their electronic configuration the lattice or crystalline field will distort and then generate an internal stress.

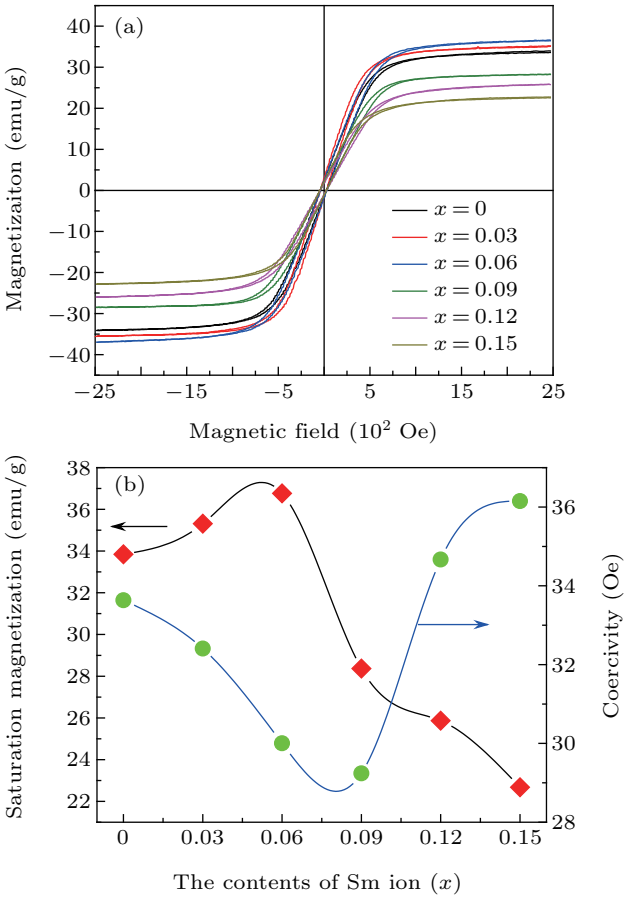


Fig. 4. The M–H loops (a) and variation in the saturation magnetization M_s and coercive field H_c of MgCd ferrite with Sm ion contents

The frequency-dependent trends of the complex magnetic permeability and dielectric permittivity for all samples, when x increases from 0 to 0.15, are shown in Fig. 5, for change in frequency ranging from 1 MHz to 1 GHz. As seen in Fig. 5(a), the real magnetic permeability (μ') remains at a stable level, and when x changes from 0 to 0.06, the real magnetic permeability of Sm-substituted Mg–Cd ferrites first increases and then decreases when $x > 0.06$. In ferrite materials, the initial permeability mainly relies on the saturation magnetization and first-order anisotropy constant (K_{u1}), and the relationship is as follows:[25]

$$\mu \propto M_s^2/(K_{u1} + \lambda_s \sigma), \tag{3}$$

where λ_s and δ represent the saturation magnetization coefficient and internal stress, respectively. In Eq. (3), the value of $\lambda_s \delta$ is so small (because of the small δ) that it can be ignored.[26,27] Therefore, a proportional trend holds between the initial permeability and M_s. In other words, permeability mainly depends on M_s. Therefore, the changing trend of M_s under different Sm^{3+} contents could account for the phenomenon of real permeability.

Considerable values (approximately 4–9 for all samples except $x = 0$) over the wide frequency range are observed in the imaginary part (μ'') of the samples in Fig. 5(a). Hence, the magnetic tangent $\tan\delta_\mu$ is obtained by the equation

$$\tan\delta_\mu = \mu''/\mu'. \tag{4}$$

Compared with other work,[28] this work renders a relatively large order of magnitude of $\tan\delta_\mu$ (approximately 3×10^{-1} to 5×10^{-2}). In addition, this work also found that the value of the imaginary part can be reduced by adding Sm^{3+}.

Figure 5(b) shows that the dielectric permittivity (ε' and ε'') of the samples depends on the Sm^{3+} doping content. The real part of the dielectric permittivity (ε') increases from 7 to 23 with Sm^{3+} content increasing from 0 to 0.15. Note that ε' displays flat responses of nearly 300 MHz. Moreover, the imaginary part of the dielectric permittivity (ε'') also has a flat response but at low values of nearly 500 MHz. For ferrite, assuming that the mechanism for electrical conduction is similar to that of dielectric polarization, the increase in dielectric permittivity can be explained. Usually, when an electric field is applied on ferrite, hence increasing the polarization, the electronic exchange between Fe^{2+} and Fe^{3+} at the octahedral sites will cause a local displacement.[29] In Mg ferrite, Sm^{3+} occupies octahedral sites (B-sites) because of its larger ionic radius and its electron configuration. The concentration of Fe^{3+} at B-sites decreases gradually with increasing Sm content. Therefore, the probability of hopping between Fe^{3+} and Fe^{2+} ions is improved, which causes the polarization to increase. Consequently, the dielectric permittivity increases with increasing Sm concentration. Moreover, material microstructure, grain size, porosity and impurities also have a great influence on the dielectric properties of materials. The grain size gradually increases then stays stable, and the density had the same trend in Figs. 3 and 2, respectively, which also increases the permittivity. In summary, all ferrite samples with $Mg_{0.8}Cd_{0.2}Fe_{2-x}Sm_xO_4$ show a constant increase in dielectric permittivity, which is consistent with other work.[28]

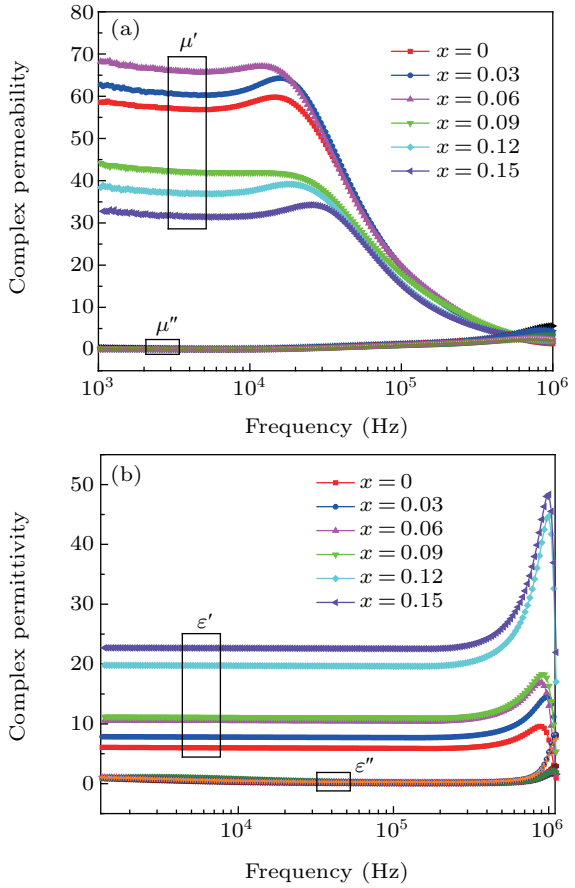


Fig. 5. Complex magnetic permeability (a) and dielectric permittivity (b) of Mg–Cd ferrites for different Sm^{3+} contents.

4. Conclusion

Sm^{3+}-substituted Mg–Cd ferrites were investigated for Sm^{3+} doping concentrations between 0 and 0.15. Phase formation and surface morphology were changed substantially. Moreover, the magnetic and dielectric properties of the spinel Mg–Cd ferrites were also studied in detail. The saturation magnetization first increases and then decreases; however, the coercivity first decreases and then increases. When $x = 0.06$, high saturation magnetization and low coercivity can be obtained. Meanwhile, the permeability and permittivity can also achieve their best values.

Acknowledgments

Project supported by the National Key Research and Development Program of China (Grant No. 2018YFE0115500), the National Natural Science Foundation of China (Grant Nos. 51902037 and 62005033), the Open Foundation of State Key Laboratory of Electronic Thin Films and Integrated Devices (Grant No. KFJJ201912), the Science and Technology Project Affiliated to the Education Department of Chongqing Municipality (Grant No. KJQN201900615), and the Nature Science Foundation of Chongqing (Grant No. cstc2019jcyj-msxmX0696).

References

[1] Hu J Y, Liu X S, Kan X C, Feng S J, Liu C C, Wang W, Urrehman K M, Shazed M, Zhou S Q and Wu Q 2019 *J. Magn. Magn. Mater.* **489** 165411
[2] Han J M, Sun L, Cao E S, Hao W T, Zhang Y J and Ju L 2021 *Chin. Phys. B* **30** 096102
[3] Yang W, Kan X C, Liu X S, Wang Z Z, Chen Z H, Wang Z, Zhu R W and Shezad M 2019 *Ceram. Int.* **45** 23328
[4] Thakur V P, Chahar D, Taneja S, Bhalla N and Thakur A 2020 *Ceram. Int.* **46** 15740
[5] Liu D, Gao S M, Jin R C, Wang F, Chu X X, Gao T P and Wang Y B 2019 *Chin. Phys. B* **28** 057503
[6] Petrov I, Niemelä M, Ponomarev P and Pyrhönen J 2017 *IEEE Trans. Indus. Electron.* **64** 5314
[7] Wu J G, Fan Z, Xiao D Q, Zhu J G and Wang J 2016 *Pro. Mater. Sci.* **84** 335
[8] Liu P J, Yao Z J and Zhou J T 2016 *Cream. Int.* **42** 9241
[9] Turchenko V, Kostishyn V G, Trukhanov S, Damay F, Porcher F, Balasoiu M, Lupu N, Bozzo B, Fina I, Trukhanov A, Waliszewski J, Recko K and Polosan S 2020 *J. Alloys Compd.* **821** 153412
[10] Heidari P and Masoudpanah S M 2020 *J. Mater. Res. Technol.* **9** 4469
[11] Nigam A and Pawar S J 2020 *Ceram. Int.* **46** 4058
[12] Kulkarni R G and Panicker V G 1984 *J. Mater. Sci.* **19** 890
[13] Akter S and Hakim M A 2010 *Mater. Chem. Phys.* **120** 399
[14] Nath S K, Maria K H, Noor S, Siker S S, Hoque S M and Hakim M A 2012 *J. Magn. Magn. Mater.* **324** 2116
[15] Gadkari A B, Shinde T J and Vasambekar P N 2009 *Mater. Charact.* **60** 1328
[16] Gadkari A B, Shinde T J and Vasambekar P N 2010 *J. Magn. Magn. Mater.* **322** 3823
[17] Kumbhar R N, Shinde T J, Kamble S A, Mathe V L and Ghodake J S 2021 *Physica B* **619** 413161
[18] Boda N, Boda G and Naidu K C B 2019 *J. Magn. Magn. Mater.* **473** 228
[19] Mohamed W S and Abu-Dief A M 2020 *Ceram. Int.* **46** 16196
[20] Bhosale J L, Kulkarni S N, Sasmile R B and Chougule B K 1996 *Bull. Mater. Sci.* **19** 767
[21] Wu X F, Ding Z, Song N G, Li L and Wang W 2016 *Ceram. Int.* **42** 4246
[22] Abdellatif M H, El-Komy G M and Azab A A 2017 *J. Magn. Magn. Mater.* **442** 445
[23] Yin Q, Liu Y, Liu Q, Wang Y, Chen J and Wang H 2019 *J. Mater. Sci: Mater. Elec.* **30** 5430
[24] Chikazumi S and Charap S 1964 *Physics of Magnetism* (John Wiley & Sons) p. 153
[25] Gan G W, Zhang D N, Li J, Wang G, Huang X, Yang Y, Rao Y H, Xu F, Wang X Y, Zhang H W and Chen R T 2020 *J. Alloys Compd.* **819** 153059
[26] Peng Y, Wu X H, Chen Z Y, Liu W H, Wang F, Wang X, Feng Z K, Chen Y J and Harris V G 2015 *J. Alloys Compd.* **630** 48
[27] Bai Y, Zhou J, Gui Z L, Li L T and Qiao L J 2008 *J. Alloys Compd.* **450** 412
[28] Li J, Wen D D, Li Q, Qiu T H, Gan G W and Zhang H W 2018 *Ceram. Int.* **44** 678
[29] Ishaque, M, Khan M A, Ali I, Khan H M, Iqbal M A, Islam M U and Warsi M F 2015 *Ceram. Int.* **41** 4028